Acta Oceanol. Sin., 2018, Vol. 37, No. 5, P. 1–7
DOI: 10.1007/s13131-018-1208-2
http://www.hyxb.org.cn
E-mail: hyxbe@263.net

Effects of surface waves and sea spray on air–sea fluxes during the passage of Typhoon Hagupit

HE Hailun[1]*, WU Qiaoyan[1], CHEN Dake[1], SUN Jia[2, 3], LIANG Chujin[1], JIN Weifang[1], XU Yao[4]

[1] State Key Laboratory of Satellite Ocean Environment Dynamics, Second Institute of Oceanography, State Oceanic Administration, Hangzhou 310012, China

[2] The First Institute of Oceanography, State Oceanic Administration, Qingdao 266061, China

[3] Laboratory for Regional Oceanography and Numerical Modeling, Qingdao National Laboratory for Marine Science and Technology, Qingdao 266061, China

[4] School of Geographic and Oceanographic Sciences, Nanjing University, Nanjing 210023, China

Received 15 November 2016; accepted 28 December 2017

Abstract

Air–sea exchange plays a vital role in the development and maintenance of tropical cyclones (TCs). Although studies have suggested the dependence of air–sea fluxes on surface waves and sea spray, how these processes modify those fluxes under TC conditions have not been sufficiently investigated based on *in-situ* observations. Using continuous meteorological and surface wave data from a moored buoy in the northern South China Sea, this study examines the effects of surface waves and sea spray on air–sea fluxes during the passage of Typhoon Hagupit. The mooring was within about 40 km of the center of Hagupit. Surface waves could increase momentum flux to the ocean by about 15%, and sea spray enhanced both sensible and latent heat fluxes to the atmosphere, causing Hagupit to absorb 500 W/m^2 more heat flux from the ocean. These results have powerful implications for understanding TC–ocean interaction and improving TC intensity forecasting.

Key words: air-sea flux, surface wave, sea spray, bulk formula, tropical cyclone

Citation: He Hailun, Wu Qiaoyan, Chen Dake, Sun Jia, Liang Chujin, Jin Weifang, Xu Yao. 2018. Effects of surface waves and sea spray on air–sea fluxes during the passage of Typhoon Hagupit. Acta Oceanologica Sinica, 37(5): 1–7, doi: 10.1007/s13131-018-1208-2

1 Introduction

Momentum and heat exchanges between the atmosphere and ocean are critical in the process of tropical cyclones' (TCs, also known as typhoons) development (Emanuel, 1988). Surface fluxes can be directly observed though turbulence-involved sensors under weak and moderate wind conditions (Gerbi et al., 2008; Li et al., 2013; Wang et al., 2013). The exchange coefficients (characterizing exchange efficiency) for sensible and latent heat fluxes are almost independent of wind (10-m neutral) speed up to 25 m/s, whereas the exchange coefficient for momentum (the drag coefficient) increases quasi-linearly with speeds up to 32 m/s (Smith, 1988). At present, direct *in-situ* measurements of air–sea turbulent fluxes are restricted to wind speeds less than 32 m/s, and these direct measurements are available from towers (Gerbi et al., 2008), buoys (Potter et al., 2015), or aircraft (French et al., 2007; Drennan et al., 2007).

Because there is no directly observed momentum flux for wind speeds greater than 32 m/s, such fluxes under strong wind conditions are generally deduced from environmental parameters that have a much lower frequency than turbulence. Through analyzing the atmospheric wind profile and computing air–sea momentum flux, Powell et al. (2003) discovered the well-known phenomenon that the surface drag coefficient levels off as wind speeds increase above 33 m/s. This phenomenon was supported by indirect estimation via oceanic measurement (Jarosz et al., 2007) and laboratory study (Donelan et al., 2004). The recent work of Potter et al. (2015) presented new evidence of a level-off at wind speeds greater than 22 m/s from direct flux measurements of a moored buoy. This result agrees with Powell et al. (2003)'s discovery, but their level-off was at a lower wind speed. Maximum 30-min sustained wind speeds recorded in Potter et al. (2015) were 26 m/s; however, under most TC conditions, speeds are greater than that. The disagreement in level-off at various wind speeds in different studies calls for further exploration of momentum flux under the strong winds of TCs.

Direct measurements of air–sea turbulent heat fluxes are even more difficult than those of momentum fluxes under strong winds. One possible reason is that the turbulence sensors of temperature and vapor are not as accurate as those of velocity fluctuations (Pedreros et al., 2003). The ONR-sponsored Coupled Boundary Layer Air–Sea Transfer (CBLAST) Hurricane Program made the first ever direct measurements of turbulent heat fluxes within a hurricane boundary layer (French et al., 2007; Drennan et al., 2007; Zhang et al., 2008). The CBLAST field observations gave sensible heat and enthalpy flux for 10-m wind speeds up to 30 m/s, which substantially extended the range of air–sea flux measurements and allowed estimation of the enthalpy exchange coefficients at wind speeds near hurricane force. However, the

Foundation item: Zhejiang Provincial Natural Science Foundation of China under contract No. LR15D060001; the National Program on Global Change and Air-Sea Interactions under contract No. GASI-IPOVAI-04; the National Natural Science Foundation of China under contract Nos 41476021, 41706034 and 41321004.
*Corresponding author, E-mail: hehailun@sio.org.cn

ratio of the exchange coefficient of enthalpy flux to the drag coefficient measured in the CBLAST field was considerably below the threshold for hurricane development suggested by Emanuel (1995) (Zhang et al., 2008).

Because many uncertainties remain in determining the surface flux in strong wind regimes, there is much room for improvement. However, in some practical circumstances, air–sea flux estimation using bulk formulae is still widely used. Surface waves and sea spray can substantially affect the exchange coefficients under TC conditions and contribute to improved air–sea flux estimation. For instance, *in-situ* observations under weak and moderate wind suggest that air–sea flux depends on surface waves (Zhao et al., 2003; Zhao and Xie, 2010). Those waves change surface dynamic roughness and are important in momentum exchange between the atmosphere and ocean (Taylor and Yelland, 2001; Oost et al., 2002; Drennan et al., 2003, 2005; He and Chen, 2011; Song et al., 2015; Zhang et al., 2016; Zhang and Song, 2018). Many scholars have investigated momentum flux under strong winds using theoretical methods. Hara and Belcher (2004) built a coupled wind–wave model by emphasizing the surface wave-induced part of air–sea momentum flux. The model is applicable to all wind conditions from weak to TCs, and the drag coefficient increases with speeds up to 50 m/s (Moon et al., 2004). The model was further improved by including wave breaking stress in the wave boundary layer (Kukulka and Hara, 2008a, b). Surface wave breaking or strong winds on the surface wave crest can generate large amounts of sea spray near the air–sea interface. Recently, from theoretical analysis, the so-called lubrication effect of sea spray explained the level-off phenomenon on the drag coefficient (Rastigejev et al., 2011; Rastigejev and Suslov, 2014). However, the theoretical model requires further validation under strong winds.

The evaporation of sea spray produces strong cooling in the layer of air within a few meters of the ocean surface, and thereby invigorates sensible heat exchange and storm intensity (Bao et al., 2000; Andreas and Emanuel, 2001). Once the 10-m wind speed over the ocean reaches about 11–13 m/s, spray-induced sensible and latent heat fluxes become substantial fractions (Andreas et al., 2008). In fact, the lack of observations under strong winds prohibited correct parameterization of sea spray.

Widely-used estimation of air–sea flux using bulk formulae was established for weak and moderate winds and then roughly extended to the strong wind condition. Major progress in the Coupled Ocean Atmosphere Response Experiment (COARE) flux algorithm included surface wave information (Fairall et al., 2003). To better understand air–sea flux and thereby model TCs, more physical processes in air–sea interaction should been taken into account (Walsh et al., 2010). Ocean-atmosphere coupled models have shown the important role of surface waves in TC development (Bao et al., 2000; Liu et al., 2011, 2012; Li et al., 2016). However, discrepancies in current surface wave models are still large under TC conditions, especially in wave period simulations (Xu et al., 2007; Montoya et al., 2013; Xu et al., 2017). Numerical models for simulating TC intensity are sensitive to the details of sea spray (Bao et al., 2000; Andreas and Emanuel, 2001; Wu et al., 2015), but accurate evaluation of the sea spray effect on air–sea fluxes requires *in-situ* observations.

The South China Sea (SCS) is frequently affected by typhoons. Recently, we deployed a moored buoy in the northern SCS and obtained continuous high-resolution meteorological observations for Typhoon Hagupit. Surface wave data were also provided by the mooring. Using this set of unique *in-situ* observations, the present study evaluates the effects of surface waves and sea spray on air–sea momentum and heat fluxes calculated by bulk formulae.

2 Data

We used best-track data from the Joint Typhoon Warning Center to describe the characteristics of Typhoon Hagupit (0818, Fig. 1). Hagupit first appeared in the western North Pacific at 1 200 UTC on 17 September 2008, and intensified as it passed through the Luzon Strait and entered the SCS. The maximum sustained wind speed of Hagupit reached 64.3 m/s (125 kn), and it eventually became a category-4 tropical cyclone (Xu et al., 2017). The moored buoy (19.5°N, 115.5°E) was on the left side of the Hagupit track. The closest approach to the typhoon track of the mooring was 33 km. Hagupit reached that location at 0513 UTC on 23 September 2008, with a radius of maximum wind of 52 km and translation speed of 8.46 m/s. The inertial period (*IP*) at the mooring site is 1.46 d.

The meteorological data from the buoy include wind speed, air pressure, relative humidity, and air temperature. Table 1 lists details of the instruments installed on the buoy, whose sensors are capable of meteorological measurement under TC conditions. These meteorological data were measured at 3 m above the sea surface. Those data were collected every 10 min and were summed into 1-h averages. Surface wave parameters including

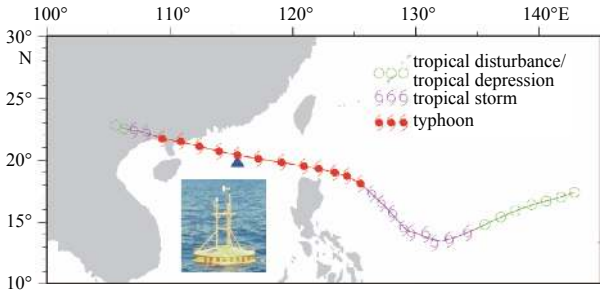

Fig. 1. Track of Typhoon Hagupit (2008) and location of moored buoy (blue triangle). Photo is of deployed buoy in northern SCS.

Table 1. Instruments installed on the buoy

Instruments	Parameter	Range	Accuray
R.M. Young, Wind Monitor 05103	wind speed	0–100 m/s	0.3 m/s
	wind direction	0°–360°	3°
Campbell Scientific, HygroClip S3	air temperature	–40–85°C	0.3°C
	relative humidity	0%–100% RH	1.5%
Vaisala, PTB100 Barometers	air pressure	500–1 100 hPa	0.3hPa@20°C
AXYS, TRIAXYS Wave Sensor	wave height	0–20 m	1%
	wave period	1.5–33 s	1%
	wave direction	0°–360°	1°

significant wave height and peak wave period were recorded once per hour, with measurement interval 20 min. SST data were not available from the buoy and were instead obtained from the AMSR-E satellite (Hilburn and Wentz, 2008). We also used 6-h cloud-cover data from NCEP reanalysis to calculate radiative fluxes.

Figure 2 shows time series of meteorological variables from the buoy. Both atmospheric and oceanic fields exhibited large variations associated with Typhoon Hagupit. The maximum meridional and zonal winds from the buoy were 25 m/s, and the corresponding maximum wind speed was 32 m/s. SST was ~29.8°C at time 2.0 *IP* before Hagupit's arrival, and cooled rapidly to 27.3°C during its passage. There was also cooling of air temperature during the typhoon forcing period. This temperature was cooler than SST before typhoon arrival, indicating that the atmosphere was receiving sensible heat flux at that time. Air pressure dropped from 1 010 to 958 hPa at typhoon arrival. The variance of relative humidity increased as Hagupit approached the mooring. Under the typhoon forcing, wave height reached 11 m, and the corresponding peak wave period was 15 s. Cloud cover increased to 90% during the typhoon forcing period.

3 Bulk formulae for air–sea fluxes

Air–sea turbulent fluxes are usually estimated through bulk formulae that are based on Monin-Obukhov similarity theory (Fairall et al., 1996, 2003; Drennan et al., 2014). These formulae calculate air–sea fluxes through multiplication of air–sea differences and exchange coefficients (Price, 1981). Those coefficients are usually parameterized using other parameters such as roughness length. We used four different algorithms to calculate the air–sea turbulence fluxes (Table 2).

The first algorithm was proposed by Large and Pond (1981, 1982; LP henceforth) based on exchange coefficient parameterizations of momentum, heat and vapor. LP is a very simple and cheap algorithm that provides baseline calculations. It has been applied in previous TC studies (Price, 1981; Moon et al., 2004). The second is the widely used flux algorithm of COARE (henceforth COR; Fairall et al., 2003), with wind-dependent roughness length parameterization. COR is different from LP in its parameterization of velocity and scalar roughness lengths (Charnock, 1955). The third is a COARE (version 3.0) algorithm with surface wave-dependent roughness length parameterization (COR-WAVE henceforth; Taylor and Yelland, 2001). COARE (version

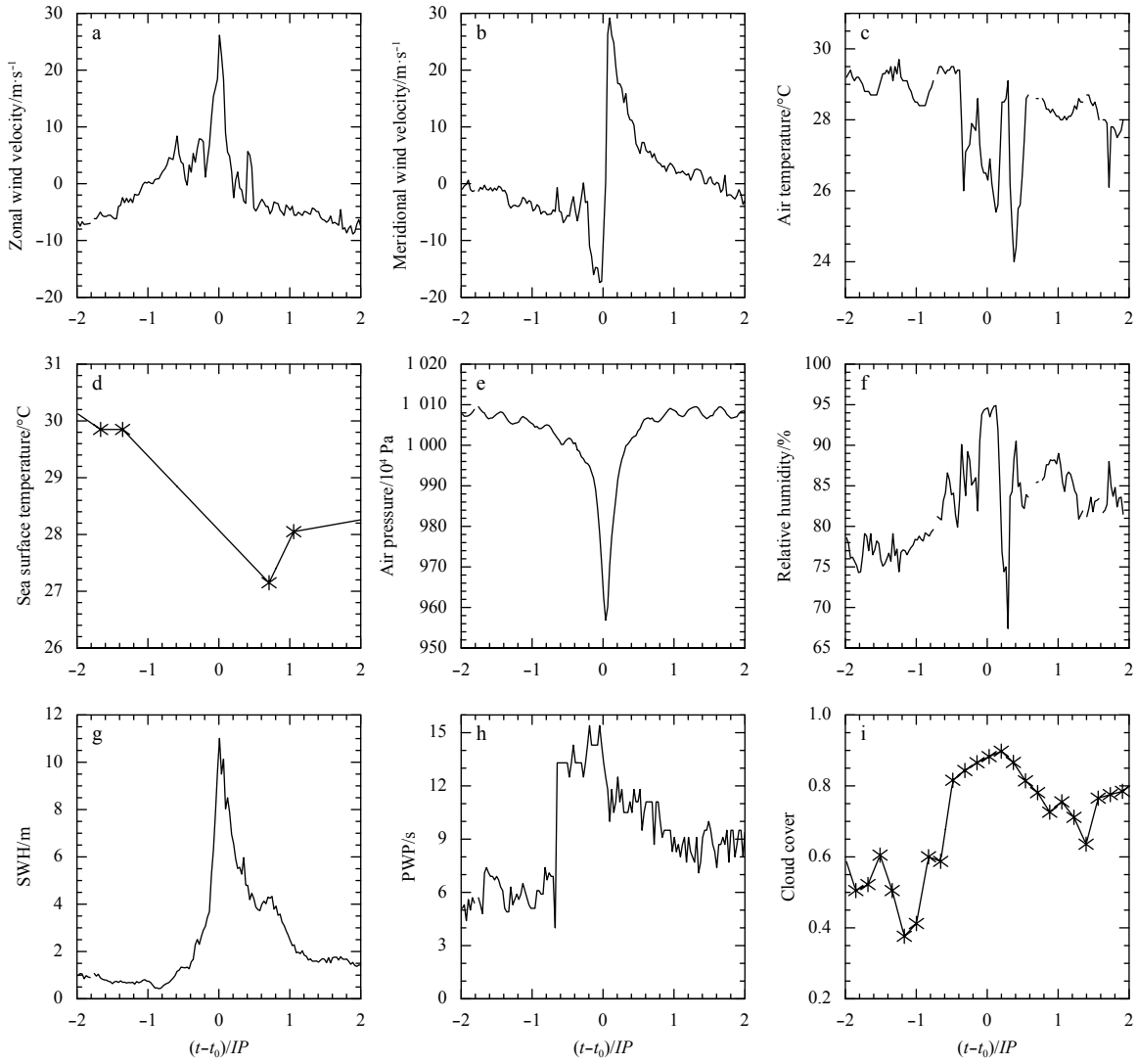

Fig. 2. Time series of meteorological variables from buoy, sea surface temperature from AMSR-E satellite, and cloud cover data from NCEP reanalysis for Typhoon Hagupit (2008). t represents time, t_0 arrival time of the typhoon, and *IP* the inertial period.

Table 2. Bulk formulae for air–sea turbulent fluxes, which include momentum flux (MF), sensible heat flux (SHF) and latent heat flux (LHF)

	MF	SHF	LHF
LP	10^3C_{dn} = 1.2, if U_{10n}<11 m/s; 10^3C_{dn} = 0.49+0.065U_{10n}, else	10^3C_{hn} =1.13	10^3C_{en} = 1.15
COR	$z_0 = 0.011\,u_*^2/g + 0.11\nu/u_*$	$z_{0T}= \nu f_T(R_r)/u_*$	$z_{0q}= \nu f_q(R_r)/u_*$
COR-WAVE	$z_0 = 1\,200h_s(h_s/L_p)^{4.5}+0.11\nu/u_*$	COR	COR
COR-SPRAY	COR	$SHF_{in}+SHF_{sp}$ SHF_{in} = COR $SHF_{sp}=\beta Q_S-(\alpha-\gamma)Q_L$	$LHF_{in}+LHF_{sp}$ LHF_{in} = COR $LHF_{sp}=\alpha Q_L$

Note: Bulk exchange coefficients for momentum, heat, and vapor are denoted by C_{dn}, C_{hn} and C_{en}, respectively, and corresponding roughness lengths are z_0, z_{0T} and z_{0q}. U_{10n} is 10-m neutral wind speed, u_* is friction velocity, ν is kinematic viscosity, g is acceleration of gravity, and R_r is the roughness Reynolds number ($R_r = z_0u_*/\nu$). $f_T(R_r)$ and $f_q(R_r)$ are functions related to SHF and LHF in COR (Fairall et al., 2003). For COR-WAVE MF, surface wave parameters include significant wave height (h_s) and peak wave period (L_p). For COR-SPRAY heat fluxes, new terms are introduced by sea spray as SHF_{sp} and LHF_{sp}, whereas some coefficients (α, β and γ) exist for adjusting physical quantities, such as Q_s (spray sensible heat flux) and Q_L (spray latent heat flux).

3.0) includes two schemes for surface wave-related roughness length. The first is wave steepness dependent (Taylor and Yelland, 2001) and the second wave age dependent (Oost et al., 2002). Under the wave age dependent schemes, when the observed wind speed is greater than 25 m/s, the bulk estimated wind stress exceeds 10 N/m², which appears unrealistic. Hence, we only used the wave steepness dependent scheme in our computation for Typhoon Hagupit. The fourth algorithm adds sea spray-related air–sea fluxes to the COARE parameterization (COR-SPRAY henceforth; Andreas et al., 2008). The Andreas et al. (2008) algorithm is basically the only one available for representing spray transfer. This algorithm uses COARE version 2.6 for interfacial flux estimation. COARE 2.6 is different from COARE 3.0 for scalar roughness lengths of winds greater than 10 m/s (Fairall et al., 1996). In the case of Typhoon Hagupit, the difference in momentum flux between versions 2.6 and 3.0 is very small (<0.05 N/m²), and differences in the maximum sensible heat and latent heat fluxes are 25.0 and 90.0 W/m², respectively.

4 Results

Figure 3a shows drag coefficients estimated from the buoy data during the passage of Hagupit (–1.5 to 1.5 *IP* relative to the arrival time). The drag coefficient from the LP scheme was independent of wind speed for weak winds (<10 m/s) but proportional to that speed for speeds greater than 10 m/s. The COR scheme shows a nearly linear correlation between the drag coefficient and wind speed for all winds. The drag coefficient from the COR-WAVE scheme was less dependent on wind speed, but in general a large drag coefficient corresponded to a strong wind. Under extremely strong winds (>30 m/s), the drag coefficient was larger with wave effects included (COR-WAVE) than without (COR or LP), consistent with Fairall et al. (2003).

Unlike in the COR and COR-WAVE schemes, the exchange coefficients of heat (Fig. 3b) and vapor (Fig. 3c) in the LP scheme were constant for all winds. Those coefficients in COR were nearly constant for wind speeds less than 10 m/s but proportional to speed for speeds greater than 10 m/s. The exchange coefficients of heat and vapor in COR were smaller than those in LP for wind speeds less than 14 m/s, but larger than those in LP for winds greater than 14 m/s. Similar to the drag coefficient, the exchange coefficients of heat and vapor in COR-WAVE were less dependent on wind speed than in the LP and COR schemes. The COR-SPRAY scheme is not included in the comparison shown in Fig. 3, because it has the same exchange coefficient as those in the COR scheme. It did not change the momentum flux but modified sensible and latent heat fluxes because of more flux terms than the exchange coefficients.

Figure 4a shows momentum fluxes calculated by all four algorithms. The evolution of these fluxes was consistent. They started to increase at 0.2 *IP* prior to typhoon arrival. As the typhoon center approached the buoy site, momentum fluxes increased rapidly. The fluxes dropped slightly immediately upon TC arrival and reached a maximum 0.1 *IP* later. Double peaks indicate the typhoon eye passed near the buoy site. The momentum fluxes from LP and COR were very similar, with a maximum of 5.4 N/m². The COR-WAVE scheme gave weaker wind stress in the period between –0.2 and 0 *IP*, but stronger from 0 to 0.2 *IP*. The maximum wind stress from COR-WAVE was 6.2 N/m², ~15%

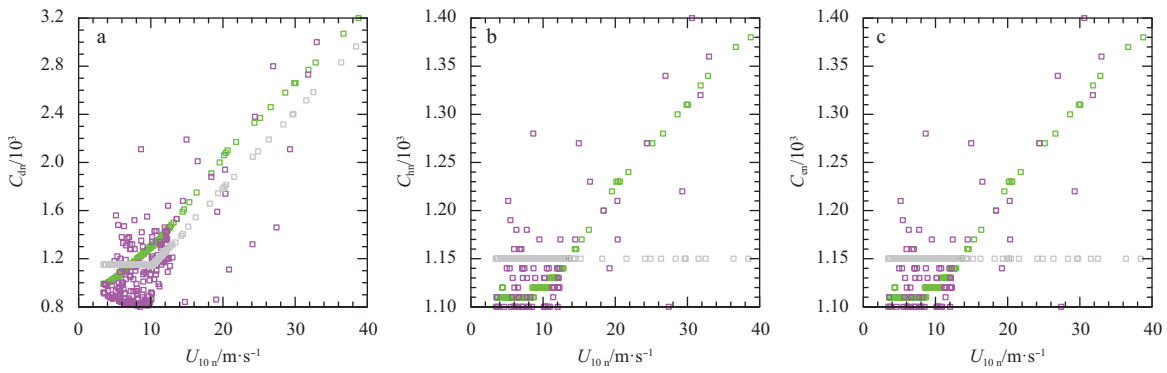

Fig. 3. Neutral exchange coefficients for momentum (C_{dn}) (a), heat (C_{hn}) (b), and vapor (C_{en}) (c) derived from buoy data for Typhoon Hagupit. U_{10n} is 10-m neutral wind speed. Grey, green and magenta squares represent LP, COR, COR-WAVE algorithms, respectively.

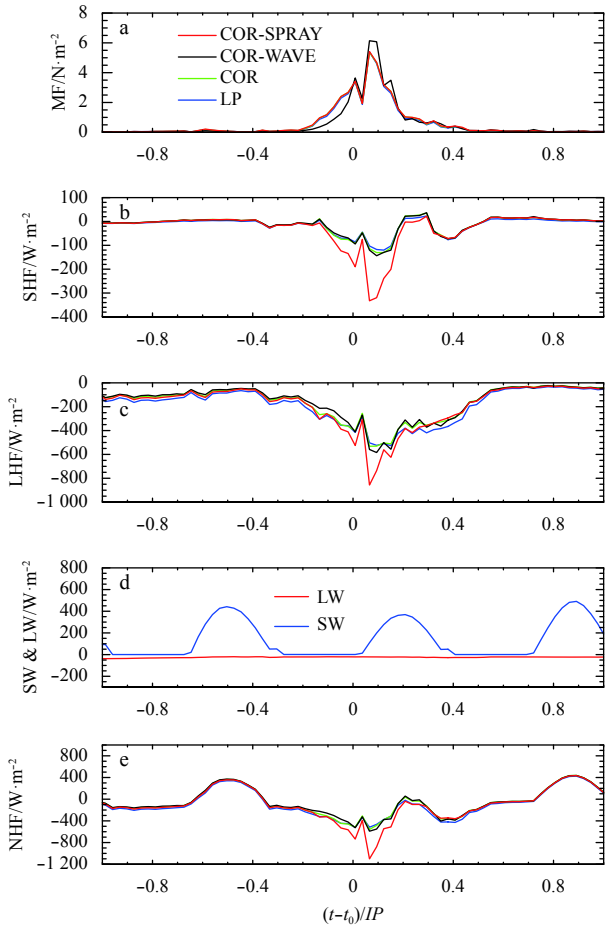

Fig. 4. Time series of air–sea flux at buoy site for Typhoon Hagupit. a. Momentum flux (MF), b. sensible heat flux (SHF), c. latent heat flux (LHF), d. net shortwave (SW) and longwave (LW) radiation, and e. net heat flux (NHF). Negative values of heat flux denote heat loss from ocean to atmosphere.

greater than that from the other three schemes.

Figure 4b shows sensible heat fluxes, in which positive (negative) values represent heat transfer from atmosphere to ocean (ocean to atmosphere). The sensible heat fluxes calculated from four different schemes had a similar evolution, apparently influenced by wind forcing. The variability of sensible heat flux was very small before 0.2 *IP* prior to typhoon arrival, and decreased by 100 W/m^2 in the subsequent 0.2 *IP*. In general, the LP, COR and COR-WAVE schemes gave similar sensible heat fluxes from ocean to atmosphere, with a maximum ~140 W/m^2. The sensible heat flux from the COR-SPRAY scheme, however, reached 340 W/m^2, more than twice that from the other three schemes. This suggests that sea spray can effectively enhance sensible heat exchange under typhoon forcing.

Latent heat fluxes (Fig. 4c) were also strongly influenced by the wind forcing. They were much greater during the typhoon forcing stage (–0.5 to 0.5 *IP*) than before typhoon arrival, and greater than the sensible heat fluxes. Latent heat loss from the ocean increased dramatically from –50 to –500 W/m^2 (LP, COR, and COR-WAVE) or –900 W/m^2 (COR-SPRAY) under the typhoon conditions. Like the sensible heat fluxes, latent heat fluxes from the LP, COR and COR-WAVE schemes were roughly the same, but including sea spray enhanced the maximum latent heat flux by 400 W/m^2.

The net heat flux (Fig. 4e) is the sum of the sensible heat, latent heat, and radiative fluxes. The latter had a distinct diurnal cycle (Fig. 4d). During the period between –0.2 and 0.2 *IP*, Hagupit had a huge heat gain from the ocean through both sensible and latent heat fluxes. Again, net heat fluxes from the LP, COR and COR-WAVE schemes were similar, with a maximum net heat flux ~600 W/m^2. The maximum was ~1 100 W/m^2 in the COR-SPRAY scheme. There was little influence of sea spray on the net heat fluxes in the period without strong winds.

5 Discussion

COARE 3.0 includes intrinsic parameterization of surface waves through wind information (Equation 27 in Fairall et al., 2003). To check the COR-WAVE parameterization in our study, surface wave parameters from the COARE 3.0 intrinsic algorithm were compared with those from *in-situ* observations, as shown in Fig. 5. The COARE 3.0 intrinsic parameterization produces wave heights as high as 40 m (in the period between –0.2 and 0.2 *IP*), which appears unrealistic (Fig. 5a). The peak wave period (Fig. 5b) from the parameterization does not reflect the wave period from observation in the period between 1 *IP* before and 1 *IP* after the typhoon. Because the parameterized wave height and wave period are substantially different from the observations, the dy-

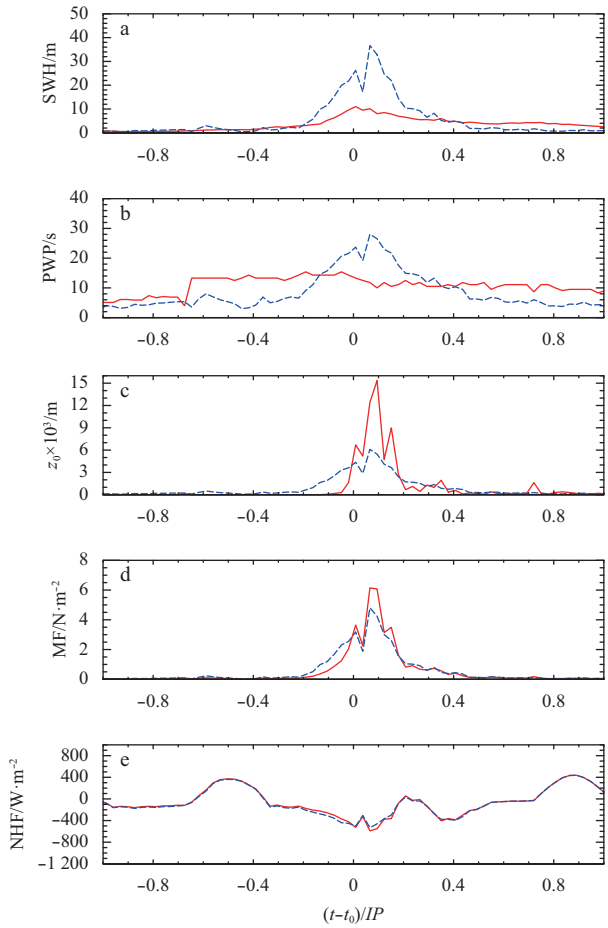

Fig. 5. Time series of wave parameters and air–sea fluxes from COARE 3.0. a. Significant wave height (SWH), b. peak wave period (PWP), c. roughness length (z_0), d. magnitude of momentum flux (MF), and e. net heat flux (NHF). Blue and red lines represent wave information from COARE 3.0 intrinsic wave parameterization and observations, respectively.

namic roughness length (denoted z_0 as shown in Fig. 5c) and corresponding momentum flux (Fig. 5d) are inconsistent with those of realistic waves during the typhoon forcing period. In detail, the dynamic roughness length is parameterized using dominant wave steepness, where that wave steepness is defined by the wave height over wavelength and the wavelength is proportional to the square of the wave period. Therefore, at TC arrival time, although the intrinsic wave parameterization produced a much higher wave height than observation, it gave an even larger wavelength, and the corresponding wave steepness and dynamic roughness length decreased but not increased. As a result, the maximum wind stress estimated from the intrinsic wave parameterization was 22% weaker than that from *in-situ* wave observation. This suggests the necessity of onsite wave observations for bulk momentum flux at typhoon forcing time. Additionally, the interfacial heat flux from the wave parameterization agrees well with that calculated from wave observation (Fig. 5e), indicating that the impact of the observed wave on that flux was relatively weak.

Bulk formulae of spray heat fluxes were parameterized based on field data, which were mostly limited to wind speeds less than 20 m/s. With such winds, the spray contribution to the joint sensible and latent heat fluxes exceeded 100 W/m^2 of the total 400 W/m^2 (Andreas and Emanuel, 2001). However, under most typhoon conditions, wind speeds are stronger than 20 m/s. For wind speeds beyond the range of flux parameterizations that have been tested, Andreas and Emanuel (2001) and Andreas et al. (2008) made extrapolation calculations using idealized analyses in which spray-mediated heat flux increases as a function of the cube of the friction velocity. In those analyses, spray sensible heat flux was ~350 W/m^2 and spray latent heat flux was ~750 W/m^2 for a 10-m wind speed of 40 m/s (Figure 8 in Andreas et al., 2008). In the case of Typhoon Hagupit, for a 10-m wind of 38 m/s (from LP algorithm), spray sensible heat flux was 200 W/m^2 and spray latent heat flux was 400 W/m^2. The underestimation in our study may be attributable to interfacial heat flux from a different version of COARE algorithm and different scenarios of air temperature, sea surface temperature, and air pressure. For instance, in Andreas et al.'s (2008) idealized analysis, air temperature, sea surface temperature, and air pressure were kept constant. These data from our *in-situ* observations varied with time.

The aforementioned level-off phenomenon of drag coefficient was examined further to determine its potential impact (Powell et al., 2003). We used Hwang's (2011) scheme, which emphasizes the concept of saturation (or level-off phenomenon) in the drag coefficient parameterization. The relative difference of momentum flux was as large as 32% when comparing Hwang's (2011) scheme with our LP (results not shown). There is no doubt that saturation effects on the drag coefficient are important and that they dominate strong-wind momentum flux. However, further exploration is beyond the scope of the present work, so we leave it to future study.

6 Concluding remarks

Taking advantage of *in-situ* observations of meteorological variables and ocean surface waves from a moored buoy, we examined the effects of surface waves and sea spray on air–sea fluxes during Typhoon Hagupit. Wind stress estimated from surface waves was 15% greater than that parameterized from wind speed in the case of Hagupit, indicating greater energy loss from typhoon to ocean. Wind stress could also enhance oceanic vertical mixing and thereby sea surface temperature cooling, further weakening the typhoon.

The effects of sea spray on air–sea fluxes were mostly on turbulent heat exchange, including both sensible and latent heat fluxes. In the case of Hagupit, accounting for sea spray increased the maximum sensible heat flux from 140 to 340 W/m^2, and the maximum latent heat flux from 500 to 900 W/m^2. The effect of sea spray resulted in Hagupit gaining 500 W/m^2 of heat flux (sum of sensible and latent heat fluxes) from the ocean. Sea spray was more important in air–sea heat exchanges than surface waves.

The present study evidences the importance of both surface waves and sea spray in typhoon–ocean interaction. The implication is that, in order to reduce uncertainties in estimating air–sea fluxes and thereby improving TC intensity forecasting, the effects of surface waves and sea spay must be properly considered. Finally, it should be noted that our evaluation of these processes was based on existing parameterizations, which need to be further validated by direct flux measurements under TC conditions.

Acknowledgements

The AMSR data are produced by Remote Sensing Systems and sponsored by the NASA Earth Science MEaSUREs DISCOVER Project and the NASA AMSR-E Science Team (www.remss.com). The NCEP Reanalysis data are provided by the NOAA/OAR/ESRL PSD (http://www.esrl.noaa.gov/psd/). The sea spray code is from Dr. E. L. Andreas (http://www.nwra.com/resumes/andreas/).

References

Andreas E L, Emanuel K A. 2001. Effects of sea spray on tropical cyclone intensity. J Atmos Sci, 58(24): 3741–3751

Andreas E L, Persson P O G, Hare J E. 2008. A bulk turbulent airsea flux algorithm for high-wind, spray conditions. J Phys Oceanogr, 38(7): 1581–1596

Bao J W, Wilczak J M, Choi J K, et al. 2000. Numerical simulations of air-sea interaction under high wind conditions using a coupled model: A study of hurricane development. Mon Weather Rev, 128(7): 2190–2210

Charnock H. 1955. Wind stress on a water surface. Q J Roy Meteor Soc, 81(350): 639–640

Drennan W M, Graber H C, Collins III C O, et al. 2014. EASI: An air-sea interaction buoy for high winds. J Atmos Ocean Technol, 31(6): 1397–1409

Drennan W M, Graber H C, Hauser D, et al. 2003. On the wave age dependence of wind stress over pure wind seas. J Geophys Res, 108(C3): 8062

Donelan M A, Haus B K, Reul N, et al. 2004. On the limiting aerodynamic roughness of the ocean in very strong winds. Geophys Res Lett, 31(18): L18306

Drennan W M, Taylor P K, Yelland M J. 2005. Parameterizing the sea surface roughness. J Phys Oceanogr, 35(5): 835–848

Drennan W M, Zhang J A, French J R, et al. 2007. Turbulent fluxes in the hurricane boundary layer: Part II. Latent heat flux. J Atmos Sci, 64(4): 1103–1115

Emanuel K A. 1988. The maximum intensity of hurricanes. J Atmos Sci, 45(7): 1143–1155

Emanuel K A. 1995. Sensitivity of tropical cyclones to surface exchange coefficients and a revised steady-state model incorporating eye dynamics. J Atmos Sci, 52(22): 3969–3976

Fairall C W, Bradley E F, Hare J E, et al. 2003. Bulk parameterization of air-sea fluxes: updates and verification for the COARE algorithm. J Climate, 16(4): 571–591

Fairall C W, Bradley E F, Rogers D P, et al. 1996. Bulk parameterization of air-sea fluxes in TOGA COARE. J Geophys Res, 101(C2): 3747–3764

French J R, Drennan W M, Zhang J A, et al. 2007. Turbulent fluxes in the Hurricane boundary layer: Part I. Momentum flux. J Atmos Sci, 64(4): 1089–1102

Gerbi G P, Trowbridge J H, Edson J B, et al. 2008. Measurements of

momentum and heat transfer across the air-sea interface. J Phys Oceanogr, 38(5): 1054–1072
Hara T, Belcher S E. 2004. Wind profile and drag coefficient over mature ocean surface wave spectra. J Phys Oceanogr, 34(11): 2345–2358
He Hailun, Chen Dake. 2011. Effects of surface wave breaking on the oceanic boundary layer. Geophys Res Lett, 38(7): L07604
Hilburn K A, Wentz F J. 2008. Intercalibrated passive microwave rain products from the unified microwave ocean retrieval algorithm (UMORA). J Appl Meteor Clim, 47(3): 778–794
Hwang P A. 2011. A note on the ocean surface roughness spectrum. J Atmos Oceanic Technol, 28(3): 436–443
Jarosz E, Mitchell D A, Wang D W T, et al. 2007. Bottom-up determination of air-sea momentum exchange under a major tropical cyclone. Science, 315(5819): 1707–1709
Kukulka T, Hara T. 2008a. The effect of breaking waves on a coupled model of wind and ocean surface waves: Part I. Mature seas. J Phys Oceanogr, 38(10): 2145–2163
Kukulka T, Hara T. 2008b. The effect of breaking waves on a coupled model of wind and ocean surface waves: Part II. Growing seas. J Phys Oceanogr, 38(10): 2164–2184
Large W G, Pond S. 1981. Open ocean momentum flux measurements in moderate to strong winds. J Phys Oceanogr, 11(3): 324–336
Large W G, Pond S. 1982. Sensible and latent heat flux measurements over the ocean. J Phys Oceanogr, 12(5): 464–482
Li Shuang, Li Ming, Gerbi G P, et al. 2013. Roles of breaking waves and Langmuir circulation in the surface boundary layer of a coastal ocean. J Geophys Res, 118(10): 5173–5187
Li Funing, Song Jinbao, He Hailun, et al. 2016. Assessment of surface drag coefficient parametrizations based on observations and simulations using the weather research and forecasting model. Atmos Oceanic Sci Lett, 9(4): 327–336
Liu Bin, Guan Changlong, Xie Li'an, et al. 2012. An investigation of the effects of wave state and sea spray on an idealized typhoon using an air-sea coupled modeling system. Adv Atmos Sci, 29(2): 391–406
Liu Bin, Liu Huiqing, Xie Lian, et al. 2011. A coupled atmosphere-wave-ocean modeling system: simulation of the intensity of an idealized tropical cyclone. Mon Weather Rev, 139(1): 132–152
Montoya R D, Arias O A, Royero O J C, et al. 2013. A wave parameters and directional spectrum analysis for extreme winds. Ocean Eng, 67: 100–118
Moon I J, Ginis I, Hara T. 2004. Effect of surface waves on Charnock coefficient under tropical cyclones. Geophys Res Lett, 31(20): L20302
Oost W A, Komen G J, Jacobs C M J, et al. 2002. New evidence for a relation between wind stress and wave age from measurements during ASGAMAGE. Bound-Layer Meteor, 103(3): 409–438
Pedreros R, Dardier G, Dupuis H, et al. 2003. Momentum and heat fluxes via the eddy correlation method on the R/V *L'Atalante* and an ASIS buoy. J Geophys Res, 108(C11): 3339
Potter H, Graber H C, Williams N J, et al. 2015. In situ measurements of momentum fluxes in typhoons. J Atmos Sci, 72(1): 104–118
Powell M D, Vickery P J, Reinhold T A. 2003. Reduced drag coefficient for high wind speeds in tropical cyclones. Nature, 422(6929): 279–283
Price J F. 1981. Upper ocean response to a hurricane. J Phys Oceanogr, 11(2): 153–175
Rastigejev Y, Suslov S A. 2014. E-ε model of spray-laden near-sea atmospheric layer in high wind conditions. J Phys Oceanogr, 44(2): 742–763
Rastigejev Y, Suslov S A, Lin Y L. 2011. Effect of ocean spray on vertical momentum transport under high-wind conditions. Bound-Layer Meteor, 141(1): 1–20
Smith S D. 1988. Coefficients for sea surface wind stress, heat flux, and wind profiles as a function of wind speed and temperature. J Geophys Res, 93(C12): 15467–15472
Song Jinbao, Fan Wei, Li Shuang, et al. 2015. Impact of surface waves on the steady near-surface wind profiles over the ocean. Bound-Layer Meteor, 155(1): 111–127
Taylor P K, Yelland M A. 2001. The dependence of sea surface roughness on the height and steepness of the waves. J Phys Oceanogr, 31(2): 572–590
Walsh K J E, Sandery P, Brassington G B, et al. 2010. Constraints on drag and exchange coefficients at extreme wind speeds. J Geophys Res, 115(C9): C09007
Wang Juanjuan, Song Jinbao, Huang Yansong, et al. 2013. Application of the Hilbert-Huang Transform to the estimation of air-sea turbulent fluxes. Bound-Layer Meteor, 147(3): 553–568
Wu Lichuan, Rutgersson A, Sahlée E, et al. 2015. The impact of waves and sea spray on modelling storm track and development. Tellus A, 67(1): 27967
Xu Yao, He Hailun, Song Jinbao, et al. 2017. Observations and modeling of typhoon waves in the South China Sea. J Phys Oceanogr, 47(6): 1307–1324
Xu Fumin, Perrie W, Toulany B, et al. 2007. Wind-generated waves in hurricane Juan. Ocean Modell, 16(3–4): 188–205
Zhang J A, Black P G, French J R, et al. 2008. First direct measurements of enthalpy flux in the hurricane boundary layer: The CBLAST results. Geophys Res Lett, 35(14): L14813
Zhang Ting, Song Jinbao. 2018. Effects of sea-surface waves and ocean spray on air-sea momentum fluxes. Adv Atmos Sci, 35(4): 469–478, doi: 10.1007/s00376-017-7101-7
Zhang Ting, Song Jinbao, Li Shuang, et al. 2016. The effects of wind-driven waves and ocean spray on the drag coefficient and near-surface wind profiles over the ocean. Acta Oceanol Sin, 35(11): 79–85
Zhao Dongliang, Toba Y, Suzuki Y, et al. 2003. Effect of wind waves on air-sea gas exchange: Proposal of an overall CO_2 transfer velocity formula as a function of breaking-wave parameter. Tellus B, 55(2): 478–487
Zhao Dongliang, Xie Lian. 2010. A practical bi-parameter formula of gas transfer velocity depending on wave states. J Oceanogr, 66(5): 663–671